Solvent induced inversion of core-shell microgels

Ali Ghavami[†] and Roland G. Winkler[*,†]

Theoretical Soft Matter and Biophysics, Institute for Advanced Simulations, Forschungszentrum Jülich GmbH, 52425 Jülich, Germany

E-mail: r.winkler@fz-juelich.de

Abstract

The morphology of core-shell microgels under different swelling conditions and as a function of the core-shell thickness ratio is systematically characterized by mesoscale hydrodynamic simulations. With increasing hydrophobic interaction of the shell polymers, we observe drastic morphological changes from a core-shell structure to an inverted microgel, where the core is turned to the outside, or a microgel with a patchy surface of core polymers directly exposed to the environment. We establish a phase diagram of the various morphologies. Moreover, we characterize the polymer and microgel conformations. For sufficiently thick shells, the changes of the shell size upon increasing hydrophobic interactions are well described by the Flory-Rehner theory. Additionally, this theory provides a critical line in the phase diagram separating core-shell structures from the distinct two other phases. The appearing new phases provide a novel route to nano- and microscale functionalized materials.

Microgels comprised of crosslinked polymers are a distinct type of smart materials. Their structures adapt to external stimuli by swelling or shrinking in response to changes in temperature, pH, ionic strength of the solution, or solvent composition.[1] This renders them ideal

candidates for a broad range of applications such as drug delivery,[2–5] sensing,[6] or food additives.[7] Even more, the possibility to change the microgel composition during the synthesis opens an avenue for novel applications. An example is the synthesis of core-shell microgels, which are typically comprised of polymers with distinctly different properties, e.g., their hydrophobicity.[8–10] While the core can accommodate different active materials the shell can be switched between a swollen or collapsed state upon an external stimulus for controlled release or uptake of molecules. Hence, recently considerable effort has been put into the development of methods for efficient and controlled manufacturing of such particles and the characterization of their internal structural properties.[8,11]

The rational design of tailored core-shell particles for specific applications requires a fundamental understanding of the detailed structural properties under different swelling conditions. Structural characterization of microgel particles is experimentally possible by scattering measurements,[12,13] however, these methods are yet unable to provide detailed morphological information, especially for highly inhomogeneous and anisotropic structures. Here, computer simulations are an excellent tool to shed light onto the structural properties of microgels. Correspondingly, a broad-range of simulation studies have been performed to investigate the swelling behavior of gels and microgels.[14–28] In particular, novel core-shell morphologies have been found by Brownian dynamics simulation in Ref. 28, with a possible "inversion" of the microgel, where core polymers are expelled from the interior. Here, we employ a hybrid simulation approach combining the multiparticle collision dynamics (MPC) method[29–31] for the fluid with molecular dynamics simulations to systematically characterize the morphologies of core-shell microgels. The simulation approach has successfully been applied to study structural and dynamical properties of a wide range of polymeric systems.[32–43] By systematically varying the hydrophobicity of shell polymers and the thickness ratio between the core and shell, we establish a phase diagram of the emerging structures and characterize the polymer and microgel conformational properties, with distinct inverse and patchy phases. Moreover, we characterize the structural properties by applying the

Flory-Rehner (FR) theory,[44–46] which has been applied successfully to describe the swelling behavior of microgels.[47–54]

Our core-shell particles are comprised of 1236 neutral, tetrafunctionally crosslinked linear polymers each with a length of $N_m = 20$ monomers. The monomers are point particles, which are connected to neighboring monomers through a harmonic potential with equilibrium bond length l. Non-bonded and hydrophobic interactions are accounted for by a Lennard-Jones potential (LJ). We consider a core-shell structure, where core monomers are in good solvent conditions. Shell monomers experience hydrophobic interactions and the solvent quality is controlled by varying the interaction parameter ε of the LJ potential. The composition of a microgel is characterized by the shell-polymer fraction $X_s = N_{\text{shell}}/N$, where N and N_{shell} are the total number of monomers and those in the shell, respectively. Further simulation details and parameters are presented in the supplementary material and Refs. 27,31,38,43.

An analytical analysis of the microgel conformations is performed by the Flory-Rehner (FR) theory. Here, the osmotic pressure of the core-shell system is given by $\pi_{\text{total}} = \pi_{\text{core}} + \pi_{\text{shell}}$.[46,55] Assuming the system is in thermal equilibrium, this equation can be solved for $\pi_{\text{total}} = 0$ to obtain the volume fraction, and hence, the radius of the microgel core and the shell. The solution method and the parameters of the model are described in the supporting information.

Simulation and analytical results for the ratio of the radius of gyration of the core $R_{\text{g,core}}$ and that of the whole microgel R_{g} are presented in Fig. 1 for various interaction strengths ε/k_BT and shell polymer fraction X_s. For microgels with large X_s, FR theory and simulations exhibit approximately the same swelling behavior, where $R_{\text{g,core}}/R_{\text{g}}$ first increases with increasing ε, passes through a maximum, and decreases again. Experimental data exhibit a similar behavior.[52] The initial increase is attributed to the fact that at low interaction strengths the shell compartment undergoes more morphological changes compared to the core compartment, while at higher interaction strengths, the core compartment also collapses resulting in a decrease of the $R_{\text{g,core}}/R_{\text{g}}$ ratio. In contrast, the simulation data

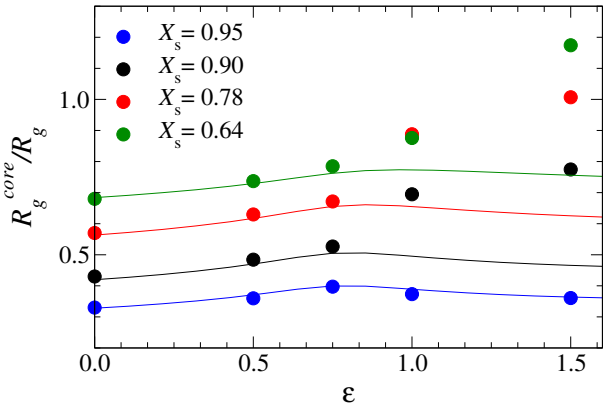

Figure 1: Ratios $R_{\mathrm{g,core}}/R_{\mathrm{g}}$ of the radius of gyration of the core and the overall R_g of the microgel obtained by simulations (filled circles) and Flory-Rehner theory (solid lines) as function of the interactions strength ε/k_BT and various shell-polymer fractions $X_s = N_{\mathrm{shell}}/N$, where N and N_{shell} are the total number of monomers and those in the shell, respectively. In case of simulations, $\varepsilon = 0$ corresponds to self-avoiding polymers, both in the shell and the core.

of core-shell microgels at smaller X_s ratios deviate from the FR prediction, and $R_{\mathrm{g,core}}/R_{\mathrm{g}}$ exhibits a strong increase with increasing ε.

The snapshots of Fig. 2 provide a hint on the observed unusual swelling behavior of the core of microgels. Interestingly, we obtain complex non-homogeneous morphologies with decreasing X_s. Aside from the conventional core-shell structure (Fig. 2a), two other morphologies emerge, namely, a microgel with an "inverted core" (Fig. 2b) and a microgel with a "patchy surface" (Fig. 2c).[28]

The dependence of the microgel's morphology on the solvent conditions can be characterized by a phase diagram (cf. Fig. 3), where we classified the various morphologies by visual inspection. For small interaction strengths or high shell volume fractions, the microgel is more or less spherically symmetric with the core fully covered by the shell. However, for certain parameters the isotropic structure breaks down and the competition between expansion of the core and contraction of the shell leads to the formation of non-homogeneous and anisotropic structures. For small X_s values, upon increasing the interaction strength, first the polymers of the shell start to form small clusters, but due to the repulsion by core monomers and geometrical restrictions by bonds, these clusters cannot merge to form a uni-

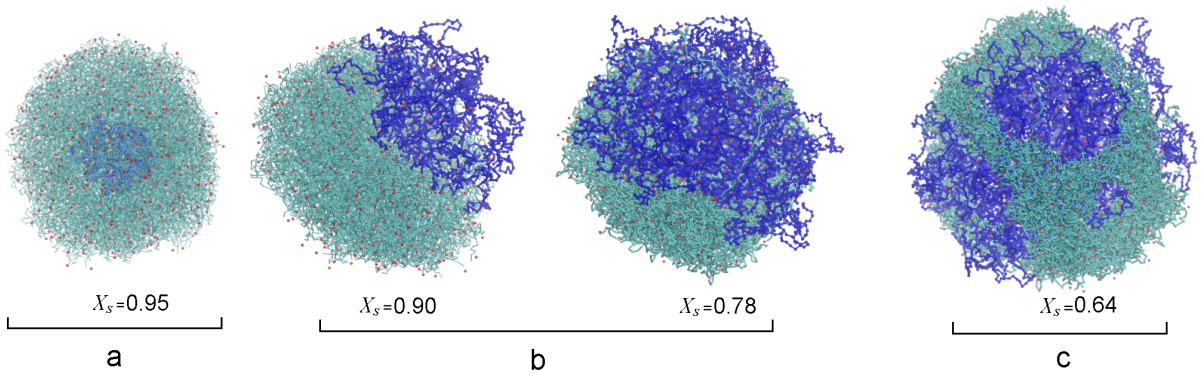

Figure 2: Snapshots of core-shell microgel morphologies for various shell polymer fractions X_s and $\varepsilon/k_BT = 1.0$. Decreasing volume fractions yield a crossover from a microgel with (a) isotropic core and shell to an (b) inverted core-shell or (c) patchy surfaces. The light-blue monomers belong to the shell, the blue monomers to the core, and red ones indicate crosslinks and chain-end monomers.

form shell, but rather form a patchy surface (see Fig 2c). A larger value of ε/k_BT implies a stronger attraction of shell polymers such that they collapse all-together and form one cluster by simultaneously expelling (part of) the core polymers (see Fig 2b for illustration). At higher ratios X_s ($X_s = 0.9$), this "core-shell inversion" happens directly without entering the patchy phase, when increasing the interaction strength.

The fact that at low X_s-values formation of an isotropic core and shell, respectively, is not simply possible at all interaction strengths suggests that the thickness of the shell should exceed a certain value to ensure a uniform coverage (i.e., no patchy surface). This is confirmed by FR theory (see Fig. 3). The dashed line in Fig. 3 shows that all the particles with a shell thickness of approximately $11.0l$ or higher form a homogeneous core-shell structure, in contrast, particles with shell thicknesses smaller than the threshold value form non-homogeneous morphologies and the predictions of the FR theory breaks down. However, the FR theory as such is unable to distinguish between patchy and inverted structures (dotted line in Fig. 3) and more advanced models are required for an analytical description. It should also be noted that the indicated critical thickness is only valid for the specific system studied here and can be different for microgels with different polymer lengths and crosslink densities.

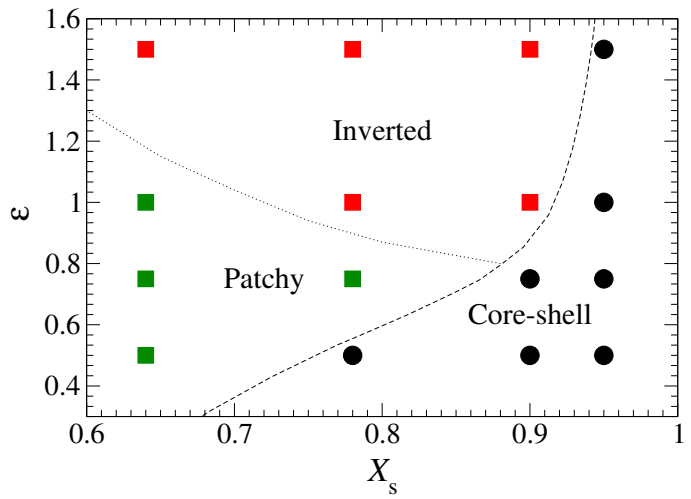

Figure 3: Phase diagram of core-shell structures in terms of the shell volume fraction X_s and interaction strength ε/k_BT. The dashed line indicates to the isoline for a thickness of $11.0l$ (see Fig. S2 in the SI) and the dotted line is a hypothetical line separating the patchy and inverted phase.

As a result of the core-shell inversion, some of the chains in the core and shell compartments are considerably stretched. To characterize the chains deformation, we calculate the distribution function of the end-to-end distance R_{ee} in the core and shell, respectively. Figure 4 presents results for $\varepsilon/k_BT = 1.0$ and various X_s values. For a homogeneous core and shell ($X_s = 0.95$), the core compartment is completely collapsed and polymers in the core and shell exhibit approximately the same mean end-to-end distance. For core-shell microgels with an inverted morphology ($X_s = 0.9$ and 0.78), a second peak at a large distance appears, which indicates that some of the polymers in both compartments are in an extended conformation. The enthalpic energy gain from the collapse of the shell compensates the entropic cost of stretching a group of polymers such that the inverted morphology is geometrically feasible. Additionally, in particles with a patchy surface ($X_s = 0.64$), polymers in the core compartment show an average end-to-end distance larger than that of polymers in the shell. The open patches allow the core polymers to explore more space and to assume more relaxed conformations (cf. Fig. 2).

The structural changes are reversible, in particular the inversion process. To confirm the reversibility, we consider an inverted state with $X_s = 0.90$ and $\varepsilon/k_BT = 1$ as starting

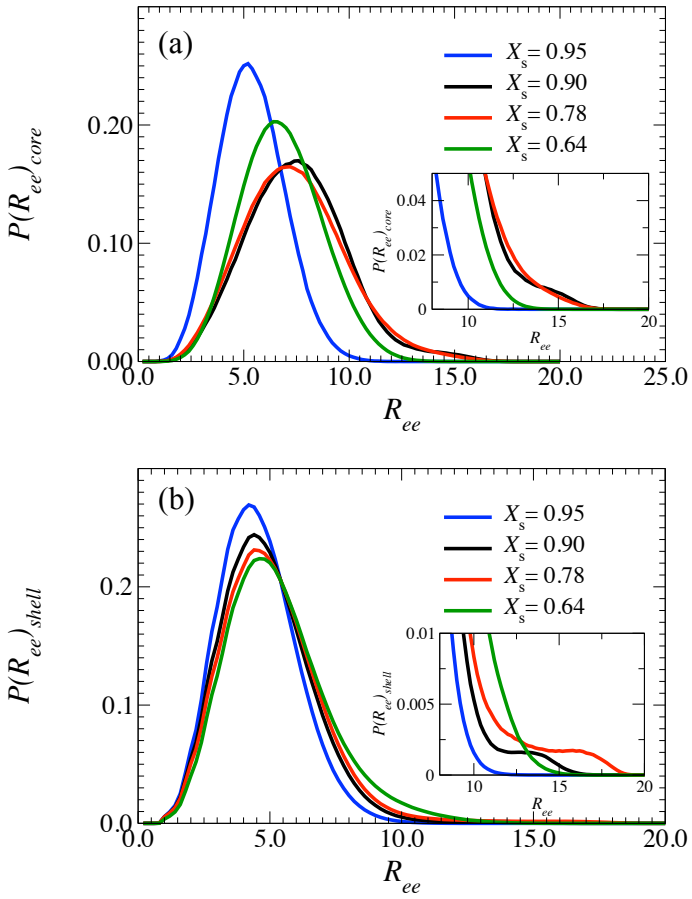

Figure 4: Distribution functions of the end-to-end distance for polymers in the (a) core and (b) shell for various shell-thickness ratios and the interaction strength of $\varepsilon/k_BT = 1.0$. (a) The nonmonotonic variation of the distribution function with X_s is a consequence of the larger conformational freedom of polymers in the inverted state ($X_s = 0.78$ and 0.9).

configuration, and then reduce the interaction strength to $\varepsilon/k_BT = 0.75$, well within the isotropic core-shell region of the phase diagram (cf. Fig. 3). Our simulations indeed show a gradual restructuring of the microgel (cf. SI movie). The core compartment is step-by-step covered by the outer polymers and the shell is reformed. The entropic part of the free energy of the shell monomers exceeds the enthalpic contributions and an isotropic core-shell microgel is formed. A subsequent increase of the interaction strength to $\varepsilon/k_BT = 1.0$ leads again to an inverted core-shell microgel (cf. SI movie). The radius of gyration of the microgel and the eigenvalues of the radius of gyration tensor during the inversion cycle are displayed in Fig. 5. The Figure indicates a two-stage process in the formation of the core-shell structure.

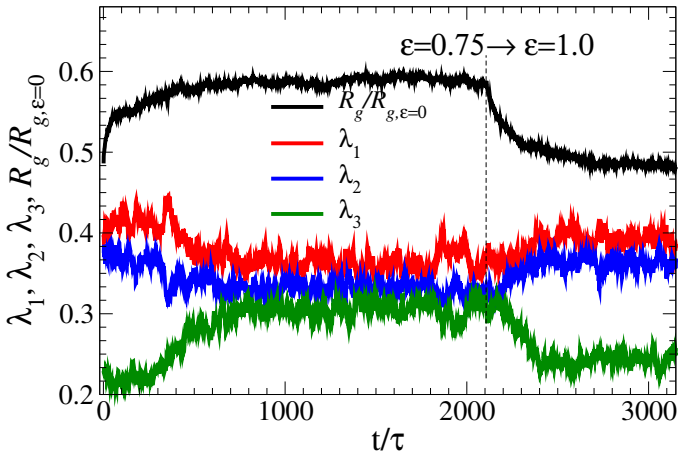

Figure 5: Reversibility of core-shell inversion process illustrated for $X_s = 0.90$. At $t = 0$, the interaction strength between core monomers is changed from $\varepsilon/k_BT = 1$ to 0.75 and, at $t/\tau = 2100$, back to 1. The black line represents the radius of gyration of the whole core-shell particle normalized by its value in swollen state. λ_1, λ_2, and λ_3 are normalized eigenvalues of the radius of gyration tensor sorted according to their magnitude. τ is the time unit of the simulation.

Quickly after changing the interaction strength from $\varepsilon/k_BT = 1.0$ to 0.75 ($0 < t/\tau \lesssim 50$), R_g increases while the eigenvalues remain essentially constant. This initial fast increase in size is due to swelling of the shell induced by the decreased attraction between the shell monomers. During the second step, in the time interval $100 \lesssim t/\tau \lesssim 800$, the radius of gyration gradually increases until a plateau value is reached. The eigenvalues, which are quite different in the inverted conformation, increase or decrease, respectively, and become rather similar as a more isotropic morphology is formed. The (average) eigenvalues are not identical at equilibrium, which reflects the fact that the structure of a microgel is fluctuating in time and is statistically never an exact sphere. Obviously, the process is reversed, when switching the interaction strength from $\varepsilon/k_BT = 0.75$ to 1.0. Here, again a two-step process occurs, with an abrupt initial collapse followed by a gradual decrease of R_g and splitting of the eigenvalues during the formation of the highly anisotropic inverted core-shell morphology. Thereby, the average initial and final radius of gyration and the respective eigenvalues are equal within the statistical accuracy of the simulation. This indicates the formation of statistically equivalent structures.

In summary, we have investigated the morphology of core-shell microgels for different swelling degrees of the shell and various thickness ratios between shell and core. We find major reversible structural changes of the core-shell morphology upon changes in the hydrophobic interactions of the shell. Both, the observed inverted structure, with the core part of the microgel particle expelled from its interior, as well as the patchy surface structure, with core parts at the outer surface, provide a novel route to functional materials. In the isotropic core-shell structure, the core is protected and shielded from the environment. By changing the environmental conditions, core chains can be exposed directly to the environment by forming anisotropic and inhomogeneous morphologies. Hence, small molecules can be released or absorbed by diffusion or reactions at functional sites may occur. Moreover, the reversibility of these structural changes, provides a route to protect the core against unfavorable environments. Naturally, the degree of morphological changes depends on the polymer length and crosslink density. For very short polymers (extremely high crosslink density), no morphological changes can be expected. Hence, variation of the polymer length provides a means to control the appearing structures. We believe that the presented mechanism for core-shell microgel morphological transitions will be beneficial in the endeavor of designing new functional materials.

Acknowledgement

This research work was supported by the Deutsche Forschungsgemeinschaft within the Sonderforschungsbereich (SFB 985) "Functional Microgels and Microgel Systems".

Supporting Information Available

Description of model and simulation approach; Solution of Flory-Rehner equation; Animation of microgel conformational changes

References

(1) Stuart, M. A. C.; Huck, W. T. S.; Genzer, J.; Müller, M.; Ober, C.; Stamm, M.; Sukhorukov, G. B.; Szleifer, I.; Tsukruk, V. V.; Urban, M.; Winnik, F.; Zauscher, S.; Luzinov, I.; Minko, S. Emerging applications of stimuli-responsive polymer materials. *Nat. Mater.* **2010**, *9*, 101–113.

(2) Berndt, I.; Pedersen, J. S.; Richtering, W. Temperature-Sensitive Core–Shell Microgel Particles with Dense Shell. *Angew. Chem.* **2006**, *118*, 1769–1773.

(3) Welsch, N.; Wittemann, A.; Ballauff, M. Enhanced activity of enzymes immobilized in thermoresponsive core- shell microgels. *J. Phys. Chem. B* **2009**, *113*, 16039–16045.

(4) Dickerson, E. B.; Blackburn, W. H.; Smith, M. H.; Kapa, L. B.; Lyon, L. A.; McDonald, J. F. Chemosensitization of cancer cells by siRNA using targeted nanogel delivery. *BMC Cancer* **2010**, *10*, 1.

(5) Bysell, H.; Månsson, R.; Hansson, P.; Malmsten, M. Microgels and microcapsules in peptide and protein drug delivery. *Adv. Drug Deliv. Rev.* **2011**, *63*, 1172–1185.

(6) Luo, Q.; Liu, P.; Guan, Y.; Zhang, Y. Thermally Induced Phase Transition of Glucose-Sensitive Core- Shell Microgels. *ACS Appl. Mater. Interfaces* **2010**, *2*, 760–767.

(7) Esser-Kahn, A. P.; Odom, S. A.; Sottos, N. R.; White, S. R.; Moore, J. S. Triggered release from polymer capsules. *Macromolecules* **2011**, *44*, 5539–5553.

(8) Berndt, I.; Pedersen, J. S.; Richtering, W. Structure of multiresponsive "intelligent" core-shell microgels. *J. Am. Chem. Soc.* **2005**, *127*, 9372–9373.

(9) Blackburn, W. H.; Lyon, L. A. Size-controlled synthesis of monodisperse core/shell nanogels. *Colloid Polym. Sci.* **2008**, *286*, 563–569.

(10) Richtering, W.; Pich, A. The special behaviours of responsive core–shell nanogels. *Soft Matter* **2012**, *8*, 11423–11430.

(11) Karg, M.; Pastoriza-Santos, I.; Liz-Marzán, L. M.; Hellweg, T. A versatile approach for the preparation of thermosensitive PNIPAM core–shell microgels with nanoparticle cores. *ChemPhysChem* **2006**, *7*, 2298–2301.

(12) Maccarrone, S.; Scherzinger, C.; Holderer, O.; Lindner, P.; Sharp, M.; Richtering, W.; Richter, D. Cononsolvency Effects on the Structure and Dynamics of Microgels. *Macromolecules* **2014**, *47*, 5982–5988.

(13) Scherzinger, C.; Lindner, P.; Keerl, M.; Richtering, W. Cononsolvency of Poly (N, N-diethylacrylamide)(PDEAAM) and Poly (N-isopropylacrylamide)(PNIPAM) Based Microgels in Water/Methanol Mixtures: Copolymer vs Core- Shell Microgel. *Macromolecules* **2010**, *43*, 6829–6833.

(14) Schneider, S.; Linse, P. Monte Carlo simulation of defect-free cross-linked polyelectrolyte gels. *J. Phys. Chem. B* **2003**, *32*, 8030–8040.

(15) Lu, Z. Y.; Hentschke, R. Computer simulation study on the swelling of a polyelectrolyte gel by a Stockmayer solvent. *Phys. Rev. E* **2003**, *67*, 061807.

(16) Mann, B. A.; Everaers, R.; Holm, C.; Kremer, K. Scaling in polyelectrolyte networks. *Europhys. Lett.* **2004**, *67*, 786.

(17) Jha, P. K.; Zwanikken, J. W.; Detcheverry, F. A.; de Pablo, J. J.; de la Cruz, M. O. Study of volume phase transitions in polymeric nanogels by theoretically informed coarse-grained simulations. *Soft Matter* **2011**, *7*, 5965–5975.

(18) Quesada-Pérez, M.; Ahualli, S.; Martín-Molina, A. Temperature-sensitive nanogels in the presence of salt: Explicit coarse-grained simulations. *J. Chem. Phys.* **2014**, *141*, 124903.

(19) Košovan, P.; Richter, T.; Holm, C. Molecular simulations of hydrogels. *Prog. Colloid Polym. Sci.* **2013**, *140*, 205–221.

(20) Košovan, P.; Richter, T.; Holm, C. Modeling of Polyelectrolyte Gels in Equilibrium with Salt Solutions. *Macromolecules* **2015**, *48*, 7698–7708.

(21) Kobayashi, H.; Winkler, R. G. Structure of Microgels with Debye-Hückel Interactions. *Polymers* **2014**, *6*, 1602–1617.

(22) Kobayashi, H.; Winkler, R. G. Universal conformational properties of polymers in ionic nanogels. *Sci. Rep.* **2016**, *6*, 19836.

(23) Kobayashi, H.; Halver, R.; Sutmann, G.; Winkler, R. G. Polymer Conformations in Ionic Microgels in the Presence of Salt: Theoretical and Mesoscale Simulation Results. *Polymers* **2017**, *9*, 15.

(24) Claudio, G. C.; Kremer, K.; Holm, C. J. Comparison of a hydrogel model to the Poisson-Boltzmann cell model. *J. Chem. Phys.* **2009**, *131*, 094903.

(25) Schroeder, R.; Rudov, A. A.; Lyon, L. A.; Richtering, W.; Pich, A.; Potemkin, I. I. Electrostatic Interactions and Osmotic Pressure of Counterions Control the pH-Dependent Swelling and Collapse of Polyampholyte Microgels with Random Distribution of Ionizable Groups. *Macromolecules* **2015**, *48*, 5914–5927.

(26) Schmid, A. J.; Dubbert, J.; Rudov, A. A.; Pedersen, J. S.; Lindner, P.; Karg, M.; Potemkin, I. I.; Richtering, W. Multi-Shell Hollow Nanogels with Responsive Shell Permeability. *Sci. Rep.* **2016**, *6*, 22736 EP.

(27) Maccarrone, S.; Ghavami, A.; Holderer, O.; Scherzinger, C.; Lindner, P.; Richtering, W.; Richter, D.; Winkler, R. G. Dynamic Structure Factor of Core–Shell Microgels: A Neutron Scattering and Mesoscale Hydrodynamic Simulation Study. *Macromolecules* **2016**, *49*, 3608–3618.

(28) Kamerlin, N.; Elvingson, C. Collapse Dynamics of Core–Shell Nanogels. *Macromolecules* **2016**, *49*, 5740–5749.

(29) Malevanets, A.; Kapral, R. Mesoscopic model for solvent dynamics. *J. Chem. Phys.* **1999**, *110*, 8605–8613.

(30) Kapral, R. Multiparticle Collision Dynamics: Simulations of complex systems on mesoscale. *Adv. Chem. Phys.* **2008**, *140*, 89.

(31) Gompper, G.; Ihle, T.; Kroll, D. M.; Winkler, R. G. Multi-Particle Collision Dynamics: A particle-based mesoscale simulation approach to the hydrodynamics of complex Fluids. *Adv. Polym. Sci.* **2009**, *221*, 1–87.

(32) Mussawisade, K.; Ripoll, M.; Winkler, R. G.; Gompper, G. Dynamics of polymers in a particle based mesoscopic solvent. *J. Chem. Phys.* **2005**, *123*, 144905.

(33) Ryder, J. F.; Yeomans, J. M. Shear thinning in dilute polymer solutions. *J. Chem. Phys.* **2006**, *125*, 194906.

(34) Frank, S.; Winkler, R. G. Polyelectrolyte electrophoresis: Field effects and hydrodynamic interactions. *EPL* **2008**, *83*, 38004.

(35) Chelakkot, R.; Winkler, R. G.; Gompper, G. Flow-Induced Helical Coiling of Semiflexible Polymers in Structured Microchannels. *Phys. Rev. Lett.* **2012**, *109*, 178101.

(36) Nikoubashman, A.; Likos, C. N. Flow-induced polymer translocation through narrow and patterned channels. *J. Chem. Phys.* **2010**, *133*, 074901.

(37) Huang, C.-C.; Winkler, R. G.; Sutmann, G.; Gompper, G. Semidilute polymer solutions at equilibrium and under shear flow. *Macromolecules* **2010**, *43*, 10107–10116.

(38) Huang, C. C.; Gompper, G.; Winkler, R. G. Effect of hydrodynamic correlations on the dynamics of polymers in dilute solution. *J. Chem. Phys.* **2013**, *138*, 144902.

(39) Ripoll, M.; Winkler, R. G.; Gompper, G. Star polymers in shear flow. *Phys. Rev. Lett.* **2006**, *96*, 188302.

(40) Fedosov, D. A.; Singh, S. P.; Chatterji, A.; Winkler, R. G.; Gompper, G. Semidilute solutions of ultra-soft colloids under shear flow. *Soft Matter* **2012**, *8*, 4109–4120.

(41) Singh, S. P.; Huang, C.-C.; Westphal, E.; Gompper, G.; Winkler, R. G. Hydrodynamic correlations and diffusion coefficient of star polymers in solution. *J. Chem. Phys.* **2014**, *141*, 084901.

(42) Winkler, R. G.; Fedosov, D. A.; Gompper, G. Dynamical and rheological properties of soft colloid suspensions. *Curr. Opin. Colloid Interface Sci.* **2014**, *19*, 594–610.

(43) Ghavami, A.; Kobayashi, H.; Winkler, R. G. Internal dynamics of microgels: A mesoscale hydrodynamic simulation study. *J. Chem. Phys.* **2016**, *145*, 244902.

(44) Flory, P. J.; Rehner Jr, J. Statistical mechanics of cross-linked polymer networks I. Rubberlike elasticity. *J. Chem. Phys.* **1943**, *11*, 512–520.

(45) Katchalsky, A.; Lifson, S.; Exsenberg, H. Equation of swelling for polyelectrolyte gels. *J. Polym. Sci.* **1951**, *7*, 571–574.

(46) Quesada-Pérez, M.; Maroto-Centeno, J. A.; Forcada, J.; Hidalgo-Alvarez, R. Gel swelling theories: the classical formalism and recent approaches. *Soft Matter* **2011**, *7*, 10536–10547.

(47) Fernandez-Barbero, A.; Fernandez-Nieves, A.; Grillo, I.; Lopez-Cabarcos, E. Structural modifications in the swelling of inhomogeneous microgels by light and neutron scattering. *Physical Review E* **2002**, *66*, 051803.

(48) Hashmi, S. M.; Dufresne, E. R. Mechanical properties of individual microgel particles through the deswelling transition. *Soft Matter* **2009**, *5*, 3682–3688.

(49) Quesada-Pérez, M.; Ramos, J.; Forcada, J.; Martín-Molina, A. Computer simulations of thermo-sensitive microgels: Quantitative comparison with experimental swelling data. *J. Chem. Phys.* **2012**, *136*, 244903.

(50) Hertle, Y.; Zeiser, M.; Hasenöhrl, C.; Busch, P.; Hellweg, T. Responsive P (NIPAM-co-NtBAM) microgels: Flory–Rehner description of the swelling behaviour. *Colloid Polym. Sci.* **2010**, *288*, 1047–1059.

(51) Lietor-Santos, J.-J.; Sierra-Martin, B.; Vavrin, R.; Hu, Z.; Gasser, U.; Fernandez-Nieves, A. Deswelling microgel particles using hydrostatic pressure. *Macromolecules* **2009**, *42*, 6225–6230.

(52) Balaceanu, A.; Verkh, Y.; Demco, D. E.; Möller, M.; Pich, A. Correlated Morphological Changes in the Volume Temperature Transition of Core–Shell Microgels. *Macromolecules* **2013**, *46*, 4882–4891.

(53) Lee, S. M.; Bae, Y. C. A cosolvency effect on tunable thermosensitive core–shell nanoparticle gels. *Soft Matter* **2015**, *11*, 3936–3945.

(54) Lu, Y.; Ballauff, M. Thermosensitive core–shell microgels: from colloidal model systems to nanoreactors. *Prog. Polym. Sci.* **2011**, *36*, 767–792.

(55) Romeo, G.; Ciamarra, M. P. Elasticity of compressed microgel suspensions. *Soft Matter* **2013**, *9*, 5401–5406.

Graphical TOC Entry